Journal of Applied Geophysics 96 (2013) 11–18

Contents lists available at SciVerse ScienceDirect

Journal of Applied Geophysics

journal homepage: www.elsevier.com/locate/jappgeo

# Fast seismic horizon reconstruction based on local dip transformation

Guillaume Zinck [a,*], Marc Donias [a,**], Jacques Daniel [a], Sébastien Guillon [b], Olivier Lavialle [a]

[a] Université de Bordeaux, IPB, Laboratoire IMS CNRS UMR 5218, 351 cours de la Libération, 33405 Talence cedex, France
[b] TOTAL CSTJF, Avenue Larribau, 64018 Pau, France

ARTICLE INFO

*Article history:*
Received 24 April 2013
Accepted 24 June 2013
Available online 3 July 2013

*Keywords:*
Seismic horizon reconstruction
Poisson equation
Fast Fourier method
Local dip transformation

ABSTRACT

We propose a fast and real-time interactive method to reconstruct a seismic horizon with respect to a set of picked input points. The reconstruction domain is subdivided in quadrilateral domains which are determined from input points while the entire horizon is obtained part-by-part by juxtaposing independent partial reconstructions. Each quadrilateral domain is mapped onto a rectangular domain on which a non-linear partial derivative equation relied on local dip is solved by an iterative process based on a Poisson equation. The key point is the transformation of the local dip which allows the carrying out of a direct Fourier method with a low computational cost.



## 1. Introduction

Seismic horizon reconstruction has become a leading method to improve seismic data interpretation and to understand geological processes. A seismic horizon is a hypersurface of a seismic image which delimits geological layers. Many recent numerical frameworks have been dedicated to the reconstruction of a unique horizon (Bienati and Spagnolini, 1998; Blinov and Petrou, 2005; Lomask and Guitton, 2006; Lomask et al., 2006; Zinck et al., 2011) as well as to the jointed reconstruction of a set of horizons (Fomel, 2010; Ligtenberg et al., 2006; Parks, 2010). Application scopes cover various domains, like flattening (Lomask and Guitton, 2006; Parks, 2010), geological model building and reservoir characterization (Hoyes and Cheret, 2011) or chrono-stratigraphic interpretation (Donias et al., 2001; Pauget et al., 2009).

Here we focus on the reconstruction of one horizon by taking into account picked points. In case of a unique point, an efficient method proposed by (Lomask et al., 2006) is based on a two-dimensional (2-D) non-linear partial derivative equation (PDE) relied on a local dip. The PDE is solved using a Gauss–Newton approach by an iterative algorithm whose crucial step is the resolution of a Poisson equation. The extension of the method to several points by Lomask and Guitton (2006) has a computational cost which is often prohibitive for large data volume. Firstly, fast algorithms to solve the Poisson equation are irrelevant. Secondly, a reestimation of the entire horizon is required when adding or displacing a point. Moreover, this global method has to be initialized with a horizon close to the solution.

In this paper, we present an alternative local method to reconstruct a horizon with respect to a set of picked input points. Based on Lomask's iterative algorithm (2006), the approach consists in a part-by-part reconstruction. The reconstruction domain is subdivided in areas on which parts of the horizon are reconstructed independently from each other while the entire horizon is obtained by juxtaposing all reconstructed parts. The approach leads to a fast and interactive reconstruction even though it is naturally suboptimal. Indeed, fast algorithms are used to solve the Poisson equation while a real-time partial (or incremental) reestimation can be carried out: only the subdomains connected to an added or displaced point need to be recalculated. The continuity of the parts of the horizon is ensured by fixing the same values on the boundaries shared by neighboring subdomains. Moreover, fixing values on all boundaries limits the largest reconstruction domain to the convex envelope of the input points.

In the case of a 2-D domain, according to Hockney (1965), a fast reconstruction can be performed on a rectangle. In the following sections, we focus on a new fast reconstruction method for domains diffeomorphic to a rectangle and here called pseudo-rectangular domains. Each pseudo-rectangular domain is mapped onto a rectangular domain through a geometrical transformation. Instead of modifying the Poisson equation as described in standard methods (Bellman and Casti, 1971; Zhong and He, 1998), the key point of our approach is the transformation of the local dip. The Poisson equation is therefore solved by a direct Fourier method which guarantees a low computational cost.

It can be noted that our approach is valid outside the seismic application scope to reconstruct explicit surfaces of finite-dimensional vector spaces such as fibrous composite images. Moreover, the local dip transformation can be extended to reconstruct implicit surfaces of finite-dimensional vector spaces (Zinck et al., 2012).

This article is organized as follows: Section 2 introduces Lomask's horizon reconstruction algorithm, Section 3 deals with the new fast

* Correspondence to: G. Zinck, Tel.: +33 540003624.
** Correspondence to: M. Donias, Tel: +33 540008418.
*E-mail addresses:* guillaume.zinck@ims-bordeaux.fr (G. Zinck), marc.donias@ims-bordeaux.fr (M. Donias).

0926-9851/$ – see front matter © 2013 Elsevier B.V. All rights reserved.
http://dx.doi.org/10.1016/j.jappgeo.2013.06.010

reconstruction method on pseudo-rectangular domains while the two last sections respectively describe the part-by-part horizon reconstruction approach and exhibit results.

## 2. Horizon reconstruction algorithm

A seismic horizon can be considered as a curved segment in a two-dimensional space or as a surface in a three-dimensional (3-D) space and is represented by a function $f$ defined on a domain $\Omega$. The function $f$ is connected (Lomask et al., 2006) to the tangent $\mathbf{p}$ of the local dip[1] by a PDE:

$$\forall \mathrm{x} \in \Omega, \quad \nabla f(\mathrm{x}) = \mathbf{p}(\mathrm{x}, f(\mathrm{x})), \tag{1}$$

where $\nabla$ denotes the gradient operator. In a 2-D (resp. 3-D) space, x denotes a one-dimensional (1-D) variable $x$ (resp. a two-dimensional variable $(x_1, x_2)$) while the local dip is a known one (resp. two)-dimensional vector giving the slope of the horizon tangent line (resp. plane) compared to the space axis $\vec{x}$ (resp. $\vec{x}_1$ and $\vec{x}_2$). The functions $f$ and $\mathbf{p}$ are respectively considered of class $C^2$ and $C^1$.

The horizon is obtained by solving a constrained optimization problem:

$$f = \arg\min_{g \in C^2} \int_\Omega ||\nabla g(\mathrm{x}) - \mathbf{p}(\mathrm{x}, g(\mathrm{x}))||^2 d\mathrm{x}, \tag{2}$$

assuming that either the horizon boundary or points belonging to the horizon are known. Eq. (2) is non-linear, thus an iterative algorithm is used to solve it (Lomask et al., 2006). The horizon is initialized with a function $f_0$ and the iterative step is made of three parts: residual computation, update term computation and updating.

- *Residual computation*:

$$\forall\ \mathrm{x} \in \Omega, \quad \mathbf{r}_k(\mathrm{x}) = \nabla f_k(\mathrm{x}) - \mathbf{p}(\mathrm{x}, f_k(\mathrm{x})). \tag{3}$$

- *Update term computation*:

$$\delta f_k = \arg\min_{g \in C^2} \int_\Omega ||\nabla g(\mathrm{x}) + \mathbf{r}_k(\mathrm{x})||^2 d\mathrm{x}. \tag{4}$$

The solution of Eq. (4) is obtained by solving a Poisson equation

$$\Delta(\delta f_k) = -\operatorname{div}(\mathbf{r}_k), \tag{5}$$

where $\Delta$ denotes the Laplace operator and div is the divergence operator. Eq. (5) is associated with conditions on a subdomain $\Omega_I$ of $\Omega$:

$$\begin{array}{l} \forall\ \mathrm{x} \in \Omega_I, \quad \delta f_0(\mathrm{x}) = f(\mathrm{x}) - f_0(\mathrm{x}) \\ \text{and} \quad \delta f_k(\mathrm{x}) = 0 \quad \forall\ k > 0. \end{array} \tag{6}$$

If the horizon boundary is known, the subdomain $\Omega_I$ corresponds to the boundary $\partial\Omega$ of $\Omega$. The problem defined by Eqs. (5) and (6) is then called boundary problem. If one or several points belonging to the horizon are known, the subdomain $\Omega_I$ corresponds to the union set of all known points. The problem defined by Eqs. (5) and (6) is then called "inner" problem.

- *Updating*:

$$\forall\ \mathrm{x} \in \Omega, \quad f_{k+1}(\mathrm{x}) = f_k(\mathrm{x}) + \delta f_k(\mathrm{x}). \tag{7}$$

[1] The tangent $\mathbf{p}$ is previously computed over the entire seismic data by estimating the gradient field. A principal component analysis (Marfurt, 2006) is used in our method while a plane-wave destruction algorithm (Fomel, 2002) is applied in the implementation of Lomask et al. (2006).

Usual stopping criteria consider the norm of the residual (Lomask et al., 2006). Moreover, a maximal number $K$ of iterations is generally fixed to ensure the algorithm stopping.

The ability to compute the update term determines the computational efficiency of the reconstruction method. On a 1-D domain and a 2-D rectangular domain, fast Fourier algorithms (Hockney, 1965) can be applied to solve boundary problems. The update term is computed in one step:

$$\delta f_k = \mathrm{FT}^{-1}\left[\frac{\mathrm{FT}[-\operatorname{div}(\mathbf{r}_k)]}{\mathrm{FT}[\Delta]}\right], \tag{8}$$

where FT and $\mathrm{FT}^{-1}$ denote respectively the Fourier transform and the inverse Fourier transform. If a unique point belonging to the horizon is known with coordinates $(\mathrm{x}^P, f(\mathrm{x}^P))$, fast algorithms can also be used by replacing condition (6) on the value of $\delta f_k$ at the known point by an equivalent condition on the mean value of $\delta f_k$:

$$\begin{array}{l} \forall\ k \geq 0, \quad <\delta f_k> = \int_\Omega \delta f_k(\mathrm{x}) d\mathrm{x} \\ \quad \text{fixed such as} \quad f_k\left(\mathrm{x}^P\right) = f\left(\mathrm{x}^P\right). \end{array} \tag{9}$$

The problem defined by Eqs. (5) and (9) is then called mean problem. However, the Fourier algorithms cannot be carried out to solve the inner problem for several known points on the aforementioned domains. Iterative methods like descent direction approaches and relaxation algorithms are therefore proposed in the literature (Polyanin, 2002). On 2-D non-rectangular domains, excepted on a disk (Swarztrauber and Sweet, 1973), all problems lead to complex matrix inversions. For pseudo-rectangular domains, an alternative method is to map the physical domain $\Omega$ onto a rectangular computational domain $\Omega'$ by introducing a diffeomorphic transformation (Bellman and Casti, 1971; Zhong and He, 1998). On the domain $\Omega'$, a differential operator with variable coefficients takes place of the Laplace operator in Eq. (5). Matrix methods to solve Eq. (5) on $\Omega'$ (Johansen and Colella, 1998; Leveque and Li, 1994) are relatively slow although they are less complex than the approaches previously described on $\Omega$ whereas Fourier algorithms are irrelevant.

## 3. Fast reconstruction on pseudo-rectangular domains

### 3.1. Local dip transformation

In this section, we present a fast horizon reconstruction on a pseudo-rectangular domain, assuming that either the horizon boundary or a unique point belonging to the horizon is known. Instead of replacing the Laplace operator in Eq. (5), the right term $-\operatorname{div}(\mathbf{r}_k)$ is modified by a local dip transformation. The boundary and mean problems can then be solved by a Fourier algorithm.

We propose to apply on Eq. (1) the diffeomorphic transformation $\mathcal{F}$ which maps the pseudo-rectangular domain $\Omega$ onto a rectangular domain $\Omega'$. The transformation is defined by:

$$\forall\ \mathrm{x} \in \Omega, \quad \begin{bmatrix} y_1 \\ y_2 \end{bmatrix} = \mathcal{F}(\mathrm{x}) = \begin{bmatrix} \mathcal{F}_1(\mathrm{x}) \\ \mathcal{F}_2(\mathrm{x}) \end{bmatrix} \in \Omega'. \tag{10}$$

The gradient field of the function $f$ is consequently relied on a vector field by a PDE:

$$\forall\ \mathrm{y} \in \Omega', \quad \nabla f(\mathrm{y}) = \mathbf{p}'(\mathrm{y}, f(\mathrm{y})), \tag{11}$$

where y denotes the 2-D variable $(y_1, y_2)$. The 2-D vector $\mathbf{p}'$ is the tangent of the transformed local dip, which gives the slope of the horizon tangent plane compared to the axis $\vec{y}_1$ and $\vec{y}_2$ of $\Omega'$. It is expressed by:

$$\mathbf{p}' = \left[J_{\mathcal{F}}{}^T\right]^{-1} \mathbf{p}, \tag{12}$$

where $J_{\mathcal{F}}$ is the transformation Jacobian matrix defined by:

$$\forall\ \mathrm{x}\in\Omega,\quad J_{\mathcal{F}}(\mathrm{x})=\begin{bmatrix}\dfrac{\partial y_1}{\partial x_1}(\mathrm{x}) & \dfrac{\partial y_1}{\partial x_2}(\mathrm{x})\\ \dfrac{\partial y_2}{\partial x_1}(\mathrm{x}) & \dfrac{\partial y_2}{\partial x_2}(\mathrm{x})\end{bmatrix} \tag{13}$$

while $T$ and $-1$ denote respectively the matrix transpose and inverse operators.

**Proof.** Derivatives on $\Omega$ and $\Omega'$ (Bellman and Casti, 1971) are connected by the relation:

$$\begin{bmatrix}\dfrac{\partial f}{\partial x_1}\\ \dfrac{\partial f}{\partial x_2}\end{bmatrix}=\left[J_{\mathcal{F}}{}^{T}\right]\begin{bmatrix}\dfrac{\partial f}{\partial y_1}\\ \dfrac{\partial f}{\partial y_2}\end{bmatrix}. \tag{14}$$

According to Eqs. (1) and (14),

$$\left[J_{\mathcal{F}}{}^{T}\right]\begin{bmatrix}\dfrac{\partial f}{\partial y_1}\\ \dfrac{\partial f}{\partial y_2}\end{bmatrix}=\mathbf{p}. \tag{15}$$

Multiplying both sides of Eq. (15) by $\left[J_{\mathcal{F}}{}^{T}\right]^{-1}$ leads to Eq. (12). □

### 3.2. Quadrilateral domain example

A quadrilateral domain is an example of pseudo-rectangular domain. The diffeomorphic transformation $\mathcal{F}$ introduced to map a quadrilateral domain onto a rectangular one is a homography defined by a $3\times 3$ matrix $H=[h_{ji}]$ (see Fig. 1). The transformation is given by:

$$\forall\ \mathrm{x}\in\Omega,\ \begin{bmatrix}\mathcal{F}_1(\mathrm{x})\\ \mathcal{F}_2(\mathrm{x})\end{bmatrix}=\begin{bmatrix}\dfrac{h_{11}x_1+h_{12}x_2+h_{13}}{h_{31}x_1+h_{32}x_2+h_{33}}\\ \dfrac{h_{21}x_1+h_{22}x_2+h_{23}}{h_{31}x_1+h_{32}x_2+h_{33}}\end{bmatrix}. \tag{16}$$

The four terms of the Jacobian are then:

$$\begin{cases}\dfrac{\partial y_1}{\partial x_1}(x_1,x_2)=\dfrac{(h_{11}h_{32}-h_{31}h_{12})x_2+h_{11}h_{33}-h_{31}h_{13}}{(h_{31}x_1+h_{32}x_2+h_{33})^2}\\ \dfrac{\partial y_2}{\partial x_1}(x_1,x_2)=\dfrac{(h_{21}h_{32}-h_{31}h_{22})x_2+h_{21}h_{33}-h_{31}h_{23}}{(h_{31}x_1+h_{32}x_2+h_{33})^2}\\ \dfrac{\partial y_1}{\partial x_2}(x_1,x_2)=\dfrac{(h_{12}h_{31}-h_{32}h_{11})x_1+h_{12}h_{33}-h_{32}h_{13}}{(h_{31}x_1+h_{32}x_2+h_{33})^2}\\ \dfrac{\partial y_2}{\partial x_2}(x_1,x_2)=\dfrac{(h_{22}h_{31}-h_{32}h_{21})x_1+h_{22}h_{33}-h_{32}h_{23}}{(h_{31}x_1+h_{32}x_2+h_{33})^2}\end{cases}. \tag{17}$$

## 4. Part-by-part reconstruction

Given a set of input points and its convex envelope Γ, we propose two subdivisions of the domain Γ which brings about a fast reconstruction: a rectangular subdivision and a quadrilateral subdivision. They consist in paving the domain Γ respectively with rectangular subdomains whose sides are parallel to the axis of the processed data basis and with non-crossed quadrilateral subdomains. The value of the horizon on the subdomain boundaries is estimated from the input points by considering them as corners of rectangles or quadrangles. As the number of corners is generally higher than the number of input points, the other corners are particular points estimated for the paving (see Fig. 2). The rectangular subdivision is the more intuitive method but according to the number and the location of the input point the reconstruction domain can be significantly smaller than the entire domain Γ and the ratio between width and height of some rectangles can be disproportionate. In this paper, we focus on the quadrangular subdivision for which Γ is totally reconstructed and the degenerated quadrangles are unusual.

Our part-by-part horizon reconstruction method consists of four steps:

1. Paving of Γ with quadrilateral domains Ω by considering the input points as corners of the domains.
2. Reconstruction of the horizon parts on the corners and along the boundary $\partial\Omega$ of Ω.
3. Reconstruction of the horizon parts on Ω.
4. Reconstruction of the entire horizon on Γ by juxtaposition of all reconstructed horizon parts.

During the first step, the input points are firstly associated by a triangulation, i.e., considered as corners of triangles included in Γ. Each triangle can then be subdivided in three quadrilateral elements by considering the center of mass as a shared corner (see Fig. 3). As a

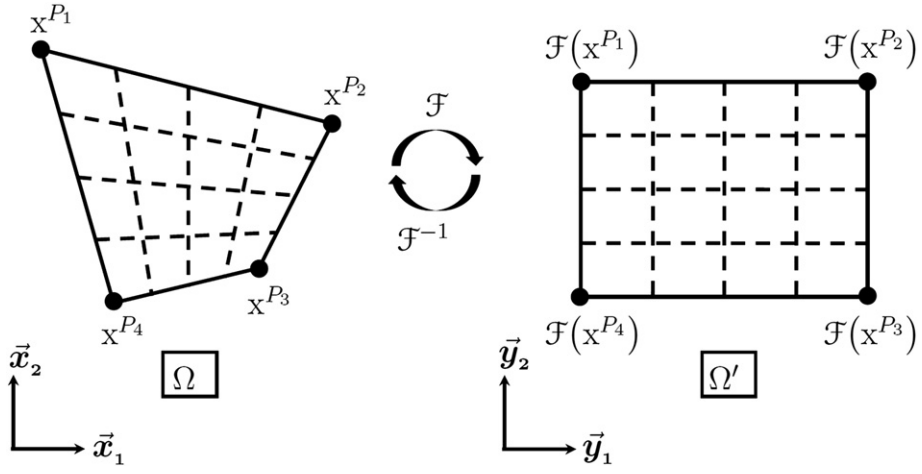


**Fig. 1.** Quadrilateral domain Ω and rectangular domain Ω′ obtained by a homography $\mathcal{F}$.

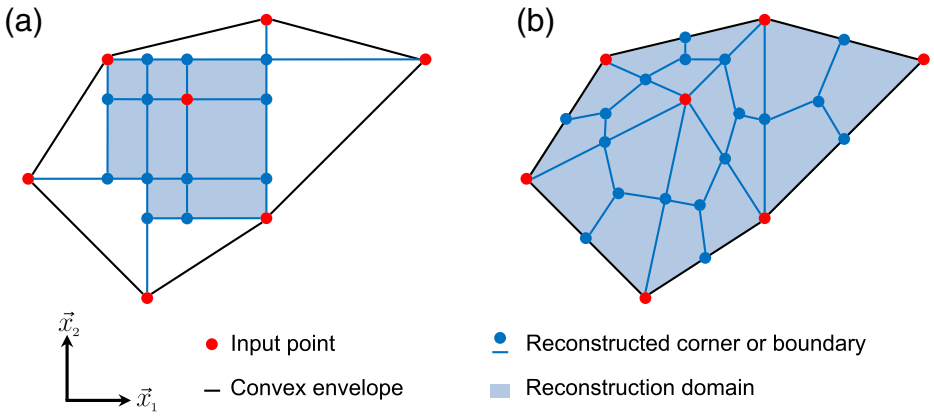


**Fig. 2.** Part-by-part reconstruction domains with respect to a set of input points (red disks): (a) rectangular subdivision; (b) quadrangular subdivision. (For interpretation of the references to color in this figure legend, the reader is referred to the web version of this article.)

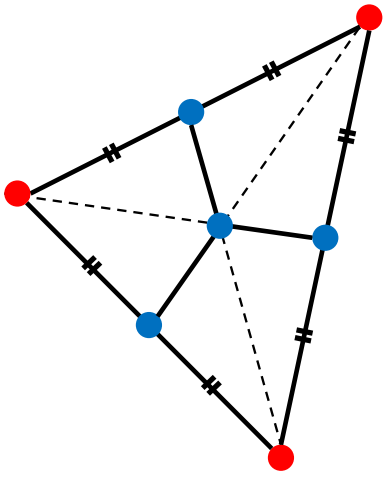

**Fig. 3.** Subdivision of a triangle in three quadrilateral elements by considering the center of mass as a shared corner.

result, the corners of the quadrangles are the input points, the midpoints of the sides and the centers of mass of the triangles while the boundaries are the sides and a part of the medians of the triangles. The choice of the triangulation of Delaunay (1934) which maximizes the smallest angle of each triangle tends to avoid skinny triangles. The triangulation requires an algorithm whose computational cost $\mathcal{O}(n \log n)$ or $\mathcal{O}(n^2)$ (de Berg et al., 2008; Lee and Schachter, 1980) depends on the number and the location of the input points. Increasing the number of quadrangles theoretically causes a lower computational time to reconstruct a horizon because the approach is based on efficient Fourier transform algorithms. Nevertheless, the cost of the boundaries' reconstructions as well as the local dip transformation becomes generally significant and the horizon quality tends to decrease.

The second step is composed of three phases. Firstly, the sides of the triangles and their midpoints are reconstructed (see Fig. 4a). Secondly, the centers of mass of the triangles are determined by estimating the medians of the triangles and their intersections. As these estimations are independent, the values of the intersections are chosen as the mean values of the three values at the centers of mass (see Fig. 4b).

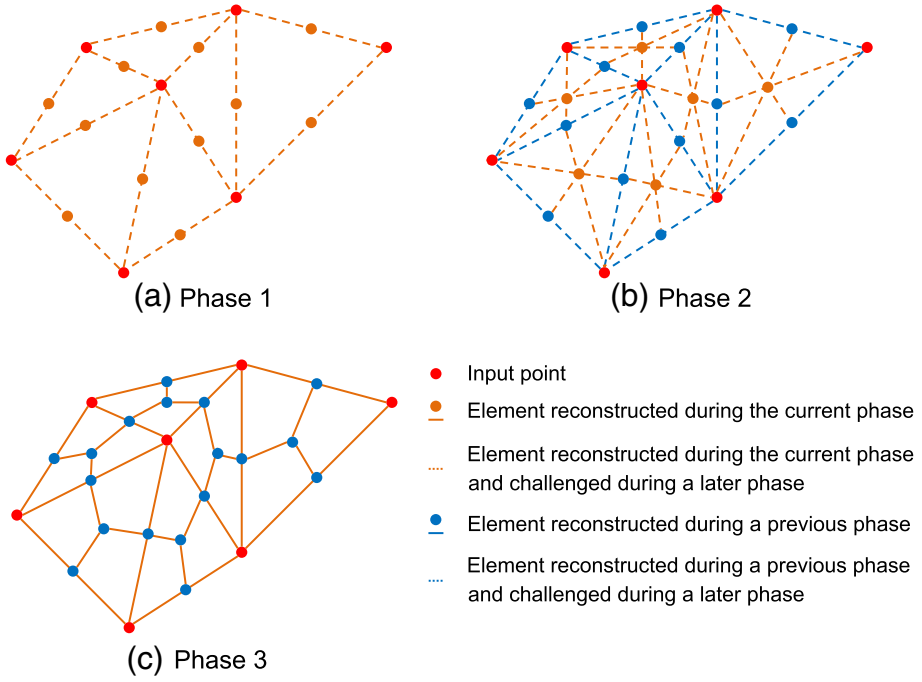


**Fig. 4.** Reconstruction of the corners and the boundaries of the quadrangles during the second step of the part-by-part method. (For interpretation of the references to color in this figure legend, the reader is referred to the web version of this article.)

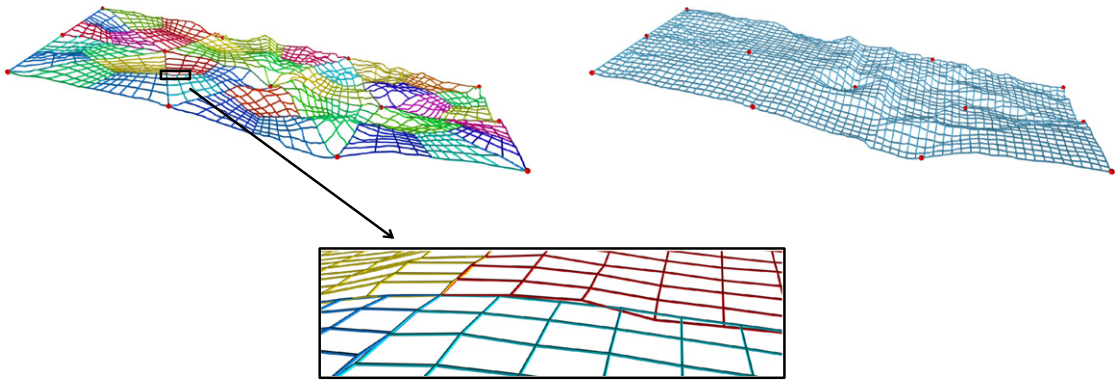

**Fig. 5.** Reconstruction of an entire horizon with respect to a set of 13 input points (red spheres) by the part-by-part method on the independent sampling grids of the quadrangles (left) and on the initial sampling grid of the reconstruction domain (right). (For interpretation of the references to color in this figure legend, the reader is referred to the web version of this article.)

Finally, the sides of the quadrangles are reconstructed (see Fig. 4c). In a numerical reconstruction, the number of sampling points of the reconstructions cannot be chosen independently of each other. In this way, the discrete lengths of the medians have to be estimated such as a sampling point matches exactly with their intersection. Moreover, because of the domain transformation, the discrete lengths of the paired opposite sides of each quadrangle have to be equal. They can be taken as the nearest integer to the shortest (Min) or the longest (Max) size as well as to their arithmetic $\left(\overline{\sum}\right)$ or geometric mean $\left(\overline{\prod}\right)$. As the method is suboptimal, this choice is a compromise between the computational cost and the data accuracy. To reduce computational cost, each considered size can be replaced by the closest size which is optimal for a fast Fourier transform algorithm, for instance the FFTW library (Frigo and Johnson, 1998).

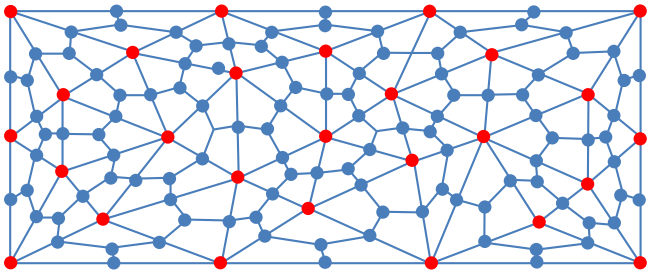

**Fig. 6.** Set of quadrangles with respect to 27 input points (red disks). (For interpretation of the references to color in this figure legend, the reader is referred to the web version of this article.)

During the third step, a loss of information results from the local dip transformation because the sampling grids of the quadrangular and of the rectangular domains are not matched.

In the fourth step, parts of the horizon are estimated on independent sampling grids of the quadrangles (see Fig. 5) which naturally do not coincide on their boundaries (see the zoom of Fig. 5). The entire horizon is then obtained either by matching the sampling grids or by estimating the horizon on the initial sampling grid of the reconstruction domain (see Fig. 5). In the first case, the reconstructions have to be resampled to ensure the same grid on the shared boundaries. The new discrete lengths are obtained by an iterative algorithm taking into account the connexity of the quadrangles and the fact that the lengths of the opposite sides have to be equal. These choices can be made during the second step but lead to a higher computational cost. In the second case, an interpolation method like the bilinear one can be used.

## 5. Results

Part-by-part and global optimization methods (Lomask and Guitton, 2006) are evaluated and compared (see Fig. 7) on real seismic data ($1000 \times 400 \times 350$). Complex geometries and convergent structures of the processed data result in an extremely noisy estimated dip, so a set of 14 input points are sequentially picked in critical regions (peaks, basins, etc.) of the horizon to be reconstructed starting from an initial set of 13 points. The number $K$ of iterations is empirically fixed to 30 to reach convergence of both methods. For the part-by-part method, the 27 input points lead to 126 quadrangles (see Fig. 6). On each subdomain, the algorithm is initialized by a constant function

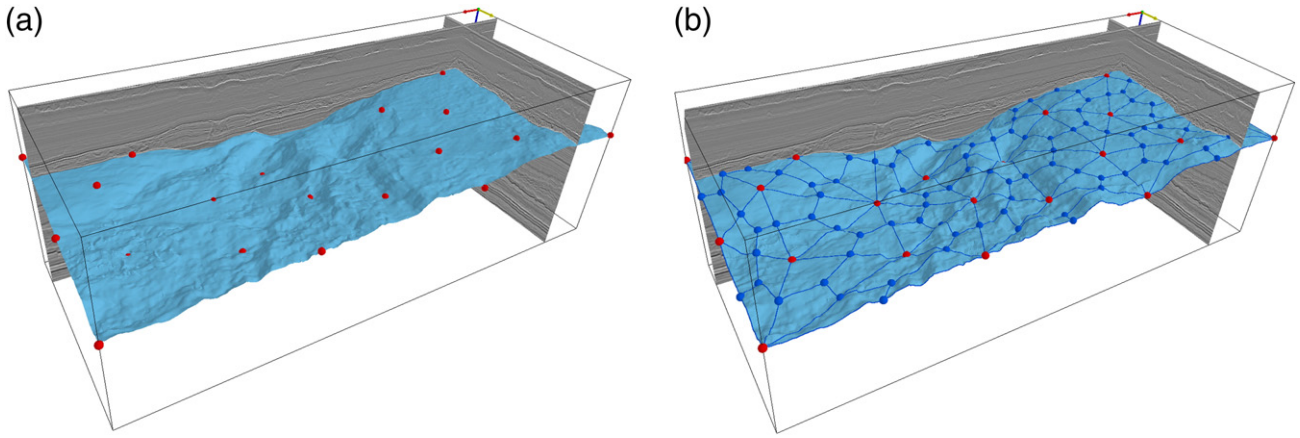


**Fig. 7.** Seismic data and reconstructed horizons with respect to a set of input points (red spheres). (a) Global optimization; (b) quadrangular subdivision. (For interpretation of the references to color in this figure legend, the reader is referred to the web version of this article.)

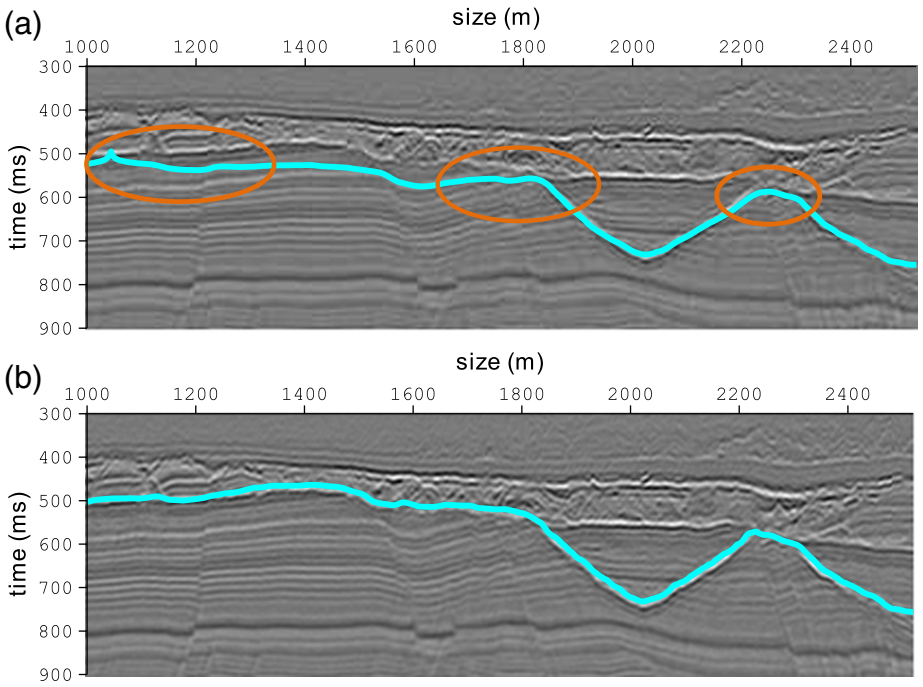


**Fig. 8.** Cross-section of the seismic data and the reconstructed horizons. (a) Global optimization; (b) quadrangular subdivision.

corresponding to the mean value of the four corners. The discrete lengths of the opposite sides are chosen equal to the nearest integer to the geometric mean $\left(\overline{\prod}\right)$ and the entire horizon is finally estimated on the initial sampling grid by a bilinear interpolation. For the global optimization method, each update term computation through a direction descent approach requires 300 iterations. The algorithm is initialized with the function proposed by Lomask and Guitton (2006) and obtained from a horizon reconstructed over the entire domain by assuming that only one particular input point is known.

### 5.1. Entire reconstruction

The reconstructed horizons for 27 input points are presented in Fig. 7. They are compared on a cross-section (see Fig. 8). The part-by-part and

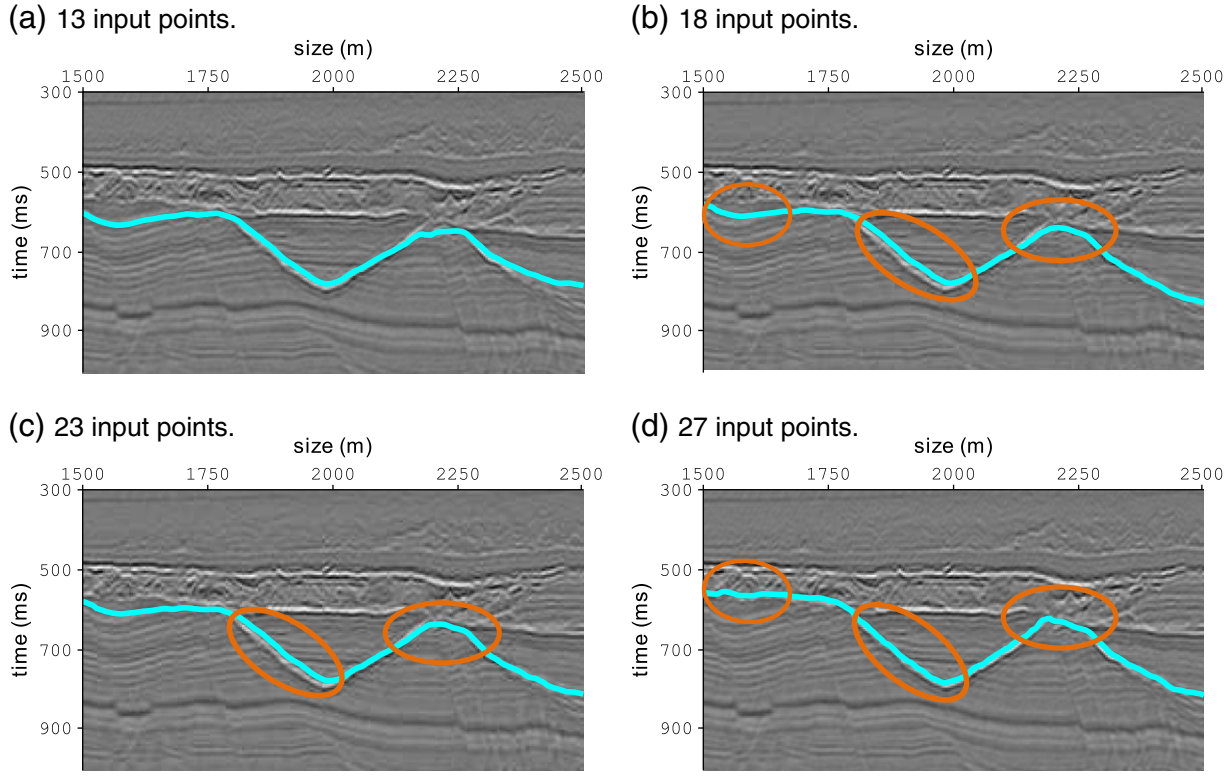


**Fig. 9.** Part-by-part reconstructed horizon versus number of input points.

**Table 1**
Computational times in seconds versus rectangular domain sizes for 27 input points. Times in parentheses are the times dedicated to the Fourier transform computations.

| Size of $\Omega'$ | Part-by-part method | | Global optimization |
|---|---|---|---|
| | Normal size | Optimal size | |
| Min | 3.3 (1.41) | 2.7 (0.561) | 79.1 |
| Max | 9.98 (5.47) | 6.43 (2.41) | |
| $\overline{\sum}$ | 5.82 (2.9) | 4.26 (1.56) | |
| $\overline{\prod}$ | 5.4 (2.54) | 3.78 (1.4) | |

**Table 2**
Computational times in seconds of the part-by-part reconstruction versus number of input points. Times in parentheses are the times dedicated to the Fourier transform computations.

| Number of input points | Entire reconstruction | Incremental reconstruction |
|---|---|---|
| 13 | 3.8 (1.4) | – |
| 18 | 3.73 (1.4) | 0.627 (0.219) |
| 23 | 3.72 (1.38) | 0.603 (0.233) |
| 27 | 3.78 (1.4) | 0.5 (0.184) |

the global optimization horizons are close to the visible horizon, which proves precision and noise robustness of both methods. Nevertheless, the global optimization horizon is not perfectly superimposed with the visible horizon on the left side, so the part-by-part method locally results in better quality horizons. The cross-sections presented in Fig. 9 depict the part-by-part horizon around the middle basin. As expected, they show that the reconstructed horizon and the visible horizon are more and more close by increasing the number of input points.

The computational cost gain of the part-by-part method is significant. For 27 input points, more than 79 s are required by the global optimization method against 5.4 s by the part-by-part method. This can principally be explained by two reasons. Firstly, the cost of the initialization step proposed by Lomask and Guitton (2006) is higher than the cost of the entire part-by-part horizon reconstruction without considering the local dip transformation step. Secondly, the update term is computed in one step in the part-by-part method whereas a large number of iterations are required in the global optimization one.

For a given number of input points, the non-fixed part of the part-by-part method computational cost mainly depends on the cost of the Fourier transform which is determined by the size of the rectangular domains. The times obtained for 27 points by considering the normal sizes Min, Max, $\overline{\sum}$ and $\overline{\prod}$ as well as the associated optimal sizes (see Section 4) are grouped in Table 1. In all cases, the cost of the part-by-part method is lower than the cost of the global optimization method, up to almost 30 times for the optimal shortest size.

### 5.2. Incremental reconstruction

Adding or displacing vertically one input point causes a reestimation of the entire horizon with the global optimization method, so the computational cost of the method does not depend on the number of input points. On the contrary, a partial (or incremental) reestimation of the horizon can be carried out with the part-by-part method: only the quadrangles connected to the added or the displaced point need to be recalculated (see Fig. 10). The costs of the entire and the incremental part-by-part reconstruction methods versus the number of points are presented in Table 2. For a given number of input points $q$, the incremental reconstruction time is the time required to estimate the horizon with respect to $q$ points knowing the horizon estimated with respect to $q-1$ points. As expected, the incremental part-by-part reconstruction is extremely fast compared to the entire reconstruction (less than 1 s) and its computational time decreases when the number of points increases. Incremental part-by-part method can consequently be considered as a real-time method which gives an interactive reconstruction of a seismic horizon.

## 6. Conclusion

We have developed a new method to reconstruct a seismic horizon with respect to a set of input points. Our approach consists in a local part-by-part reconstruction on quadrilateral subdomains. Presented as an alternative of a time-consuming global optimization method, it allows a fast and real-time interactive reconstruction. The key point is the transformation of the estimated local dip instead of the derivatives to solve a Poisson equation with a direct Fourier method which guarantees a low computational cost. The horizons obtained for real seismic data prove accuracy and noise robustness of the method. They are close to the visible ones and to those reconstructed by the global optimization method. Moreover, the observed computational time gains are extremely significant for large data volume.

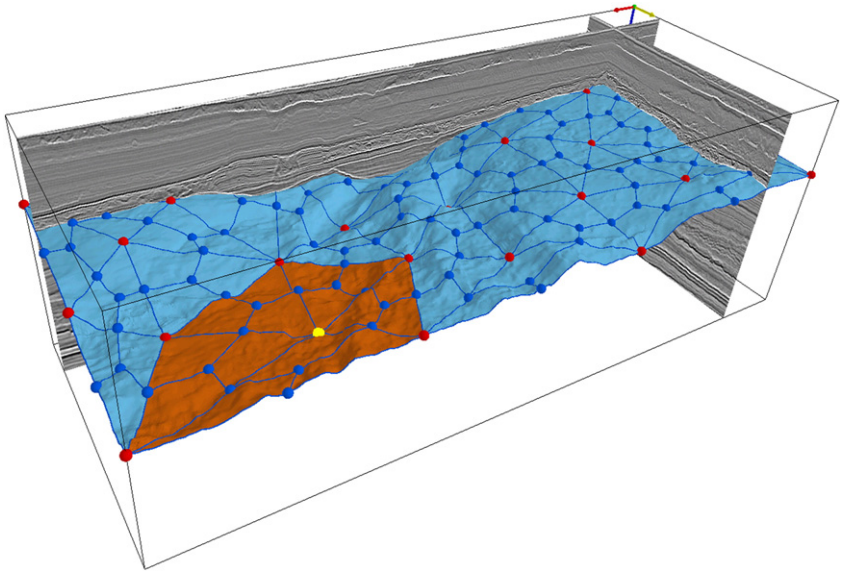

**Fig. 10.** Part-by-part reconstructed horizon with respect to a set of 27 input points (red spheres). Only the orange quadrangles are recalculated when displacing the yellow point. (For interpretation of the references to color in this figure legend, the reader is referred to the web version of this article.)

## Acknowledgments

The authors thank Total Company for supporting this work, supplying seismic data and adding the implementation of their approach in the seismic interpretation platform Sismage™.

## References

Bellman, R., Casti, J., 1971. Differential quadrature and long-term integration. Journal of Mathematical Analysis and Applications 34 (2), 235–238.
Bienati, N., Spagnolini, U., 1998. Traveltime picking in 3-D data volumes. Extended Abstracts, Session: 1–12. 60th EAGE Meeting, pp. 98–112.
Blinov, A., Petrou, M., 2005. Reconstruction of 3-D horizons from 3-D seismic datasets. IEEE Transactions on Geoscience and Remote Sensing 43 (6), 1421–1431.
de Berg, M., Cheong, O., van Kreveld, M., Overmars, M., 2008. Computational Geometry: Algorithms and Applications. Springer.
Delaunay, B., 1934. Sur la sphère vide. A la mémoire de Georges Voronoi. Bulletin de l'Académie des Sciences de l'URSS. Classe des sciences mathématiques et na, 6, pp. 793–800.
Donias, M., Guillon, S., Baylou, P., Pauget, F., Keskes, N., 2001. Method of chrono-stratigraphic interpretation of a seismic cross section or block. Elf Exploration Production, Patent US 0036294.
Fomel, S., 2002. Applications of plane-wave destruction filters. Geophysics 67 (6), 1946–1960.
Fomel, S., 2010. Predictive painting of 3D seismic volumes. Geophysics 75 (4), 25–30.
Frigo, M., Johnson, S.G., 1998. FFTW: an adaptive software architecture for the FFT. International Conference on Acoustics, Speech and Signal Processing (ICASSP). IEEE, pp. 1381–1384.
Hockney, R., 1965. A fast direct solution of Poisson's equation using Fourier analysis. Journal of the ACM 12 (1), 95–113.
Hoyes, J., Cheret, T., 2011. A review of "global" interpretation methods for automated 3-D horizon picking. The Leading Edge 30 (1), 38–47.
Johansen, H., Colella, P., 1998. A cartesian grid embedded boundary method for Poisson's equation on irregular domains. Journal of Computational Physics 147 (1), 60–85.
Lee, D.T., Schachter, B.J., 1980. Two algorithms for constructing a Delaunay triangulation. International Journal of Parallel Programming 9 (3), 219–242.
Leveque, R., Li, Z., 1994. The immersed interface method for elliptic equations with discontinuous coefficients and singular sources. SIAM Journal on Numerical Analysis 31 (4), 1019–1044.
Ligtenberg, H., de Bruin, G., Hemstra, N., Geel, C., 2006. Sequence stratigraphic interpretation in the Wheeler transformed (flattened) seismic domain. Extended Abstract. 68th EAGE Meeting.
Lomask, J., Guitton, A., 2006. Flattening with geological constraints. Annual Meeting Expanded Abstracts. Society of Exploration Geophysicists (SEG), pp. 1053–1056.
Lomask, J., Guitton, A., Fomel, S., Claerbout, J., Valenciano, A., 2006. Flattening without picking. Geophysics 71 (1), 13–20.
Marfurt, K., 2006. Robust estimates of 3-D reflector dip and azimuth. Geophysics 71 (4), 29–40.
Parks, D., 2010. Seismic Image Flattening as a Linear Inverse Problem. Colorado School of Mines.
Pauget, F., Lacaze, S., Valding, T., 2009. A global approach in seismic interpretation based on cost function minimization. Annual Meeting Expanded Abstracts. Society of Exploration Geophysicists (SEG), pp. 2592–2596.
Polyanin, A.D., 2002. Handbook of Linear Partial Differential Equations for Engineers and Scientists. Chapman & Hall/CRC.
Swarztrauber, P., Sweet, R., 1973. The direct solution of the discrete Poisson equation on a disk. SIAM Journal on Numerical Analysis 10 (5), 900–907.
Zhong, H., He, Y., 1998. Solution of Poisson and Laplace equations by quadrilateral quadrature element. International Journal of Solids and Structures 35 (21), 2805–2819.
Zinck, G., Donias, M., Guillon, S., Lavialle, O., 2011. Discontinuous seismic horizon tracking based on a Poisson equation with incremental Dirichlet boundary conditions. International Conference on Image Processing (ICIP). IEEE, pp. 3385–3388.
Zinck, G., Donias, M., Lavialle, O., 2012. N-dimensional surface reconstruction from a noisy normal vector field. European Signal Processing Conference (EUSIPCO). EURASIP, pp. 395–399.